不同组织超细化预处理下的异种钢超塑焊接

张柯柯[1], 杨蕴林[1], 赵 宁[2], 王长生[1], 王要利[1]
(1.河南科技大学 材料科学与工程学院, 河南 洛阳 471003; 2.西安交通大学 材料科学与工程学院, 西安 710049)

摘 要: 通过对 40Cr/T10A钢试样及试样待焊面表层分别实施盐浴加热循环淬火、高频淬火及激光淬火的组织超细化预处理, 探讨了钢待焊表面组织对 40Cr/T10A异材恒温超塑焊(ISSW)工艺及接头质量的影响。试验结果表明, 钢待焊表面组织对 ISSW接头的形成有重要影响。待焊面组织越细, ISSW所需焊接温度向低温区移动, 初始应变速率向高应变速率区域移动, ISSW所需时间越短; 即使待焊双方一方实施组织超细化, 也可实现接头抗拉强度达到 40Cr母材的强度, 但 ISSW所需压接时间稍长。ISSW属小变形焊接, 接头变形主要集中在原界面附近的淬火区, 且 T10A侧的变形均大于 40Cr侧。

关键词: 钢; 组织超细化; 超塑焊接; 工艺; 接头质量
中图分类号: TG453.9 文献标识码: A 文章编号: 0253-360X(2006)01-37-04

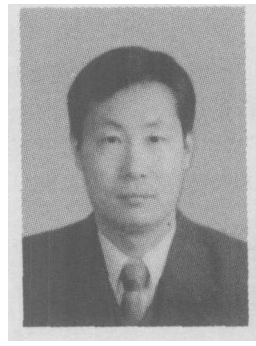

张柯柯

0 序 言

固态焊接头区不经熔化与凝固过程, 更易实现与母材组织性能一致的高质量连接, 这将成为 21世纪有重要发展的连接技术[1]。恒温超塑性焊接(ISSW)作为一种材料固态连接新技术, 其工艺设备简单, 易于实现精密焊接, 并可与塑性成形同步, 这是现有压力焊接技术所不能比拟的, 已成为近年来固态焊接非常活跃的研究领域, 尤其是超塑成形/扩散连接(SPF/DB)在航空、航天、军工等行业的应用已带来了巨大的经济效益, 成为航空航天制造业中无可替代的关键技术[2]。尽管人们对一些机械基础件材料的 ISSW工艺及接头形成过程进行了研究, 如结构钢/工具钢刀具、钢/铜合金发动机柱塞泵、钢/钛合金仪表元器件及铜合金/钨合金电触头等的 ISSW[3~7]。但有关待焊材料组织在固态焊接过程中的作用却鲜见文献报道, 这严重地制约着对固态焊本质的认识及固态焊新技术的开发。结构钢(如 40Cr)/工具钢(如 T10A)采用一般熔焊方法难以获得良好的焊接接头。为此, 作者以 40Cr/T10A ISSW为例, 探讨待焊面组织对其 ISSW的影响, 以期为高质量 ISSW新方法的开发提供理论依据。

收稿日期: 2005-02-28
基金项目: 河南省自然科学基金资助项目(0511050800); 河南省教育厅自然科学基金资助项目(2004430211); 河南省高校创新人才基金资助项目(教高 2004-294); 河南省高校杰出科研人才创新工程项目(2004KYCX020)

1 试验材料及方法

试验用 40Cr和 T10A钢为国产热轧退火态棒材, 化学成分见表 1, 40Cr显微组织为珠光体+铁素体, T10A为细粒状珠光体, 制成 φ15mm×25mm的试样。

表 1 试验用钢的主要化学成分(质量分数, %)
Table 1 Chemical compositions of steels

钢号	C	Mn	Si	Cr
40Cr	0.37~0.45	0.5~0.8	0.17~0.37	0.8~1.1
T10A	0.95~1.04	≤0.40	≤0.35	—

采用快速加热相变淬火方法在试验用钢试样表面获得 ISSW所需的超细化非平衡组织薄层。其中, 整体盐浴加热循环淬火(SCQ), 40Cr经 820℃循环淬火 2次, T10A经 780℃循环淬火 3次, 淬火后在 200℃回火 30~35min; 高频表面淬火(HFH)是在 GP100-3型高频感应加热装置上进行, 淬火介质为聚乙烯醇水溶液, 淬火后经 2 000℃回火 30~35min; 激光表面淬火(LH)采用 5kW的 CW-CO_2激光器, 光斑直径为 3mm, 搭接量为 1mm, 40Cr扫描速度为 3×10^{-2} m/s, 功率为 1 200W, T10A扫描速度为 1×10^{-2} m/s, 功率为 900W, 淬火后经 200℃回火 30~35min。经检测, 超细化预处理后试样表面和心部均获得回火马氏体, 原奥氏体晶界用过饱和苦味酸钠溶液浸蚀显示, 用截线法[8]

测得其晶粒平均截线长如表 2所示。显然,经 HFH预处理后有更好的细化效果。将经超细化预处理或未处理的待焊面磨光(表面粗糙度 $Ra<1\ \mu m$)并清洗干净,配对(40Cr/T10A异材)对接置于压头速度可在 0.05~3.5 mm/min范围内连续可调的压接装置内,并施加 $\sigma_0=56.6$ MPa预压应力。用控温精度为 ±2 ℃的 3 kW电炉加热至焊接温度保温 10 min,在适宜初始应变速率下经短时压接后卸载空冷。

表 2 奥氏体晶粒平均截线长

Table 2 Average transversal length of austenite grain

预处理工艺	钢号	奥氏体晶粒平均截线长 $l/\mu m$
整体盐浴加热循环淬火	40Cr	9.87
	T10A	8.63
高频表面淬火	40Cr	7.18
	T10A	6.72

将焊后的试样加工成 ϕ5 mm × 25 mm 拉伸试样,在 WE-300材料试验机上进行接头抗拉强度试验。用金相显微镜及 H-800透射电镜对焊接区进行显微组织观察和分析。

2 试验结果及分析

2.1 焊接变形特点

40Cr/T10A ISSW焊后试样宏观形貌如图 1所示。由图 1可见,ISSW压接后在靠近原界面处接头均发生鼓形变形,T10A侧具有较大的径向变形(膨胀率);与经 SCQ后压接试样变形有所不同,待焊面表层经 HFH和 LH后的压接试样变形主要集中在接头区附近,其余部位变形甚微;单侧经 HFH和 LH后焊接试样的变形仅表现在近界面处预处理侧略有凸起。与 40Cr/T10A真空扩散焊接约 1%的焊接变形相比,ISSW变形较大,但明显小于变形焊。因此,ISSW应属于低温小变形焊接。

2.2 焊接工艺参数

大量试验结果表明,压接双方或单方经超细化预处理(包括 SCQ、HFH和 LH)的 40Cr/T10A ISSW焊后拉伸试样,拉伸试验中大部分断在原界面处。若焊接工艺参数合适,则断口一般都断在距界面较远(4~5mm以外)的 40Cr母材一侧,反映出接头抗拉强度已达到甚至高于 40Cr母材的强度,其宏观断口呈典型的韧性断裂的杯锥状,微观形貌以韧窝特征为主。

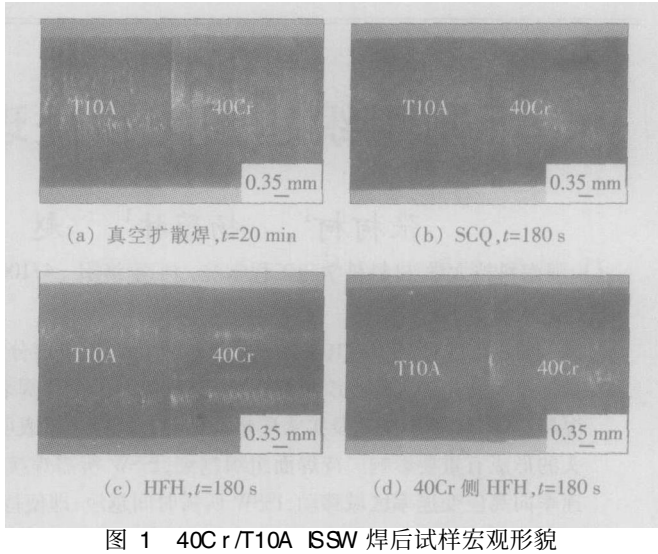

图 1 40Cr/T10A ISSW焊后试样宏观形貌

Fig. 1 Macro appearance of specimen after ISSW

基于组织超塑性的 ISSW,焊前钢的组织由于影响材料的超塑性而影响焊接效果。具有不同组织超细化效果的 SCQ、HFH、LH三种预处理工艺对 ISSW主要工艺参数的影响如下。

焊接温度,一般将压接双方的超塑性温度重叠区间作为其焊接温度,适宜的焊接温度既要满足金属超塑性流变的要求又要兼顾原子的扩散。焊接温度与接头强度的关系见图 2。由图 2可见,预处理后组织细化效果愈好,则达到 40Cr钢母材强度(经 HFH和 LH预处理 ISSW焊后 40Cr基材抗拉强度为 560~570 MPa)的 ISSW所需的温度向低温区移动。经 SCQ预处理的焊接接头抗拉强度要明显高于经 HFH和 LH预处理的抗拉强度约 100 MPa,主要是由于前者整个试样具有淬火+高温回火态的

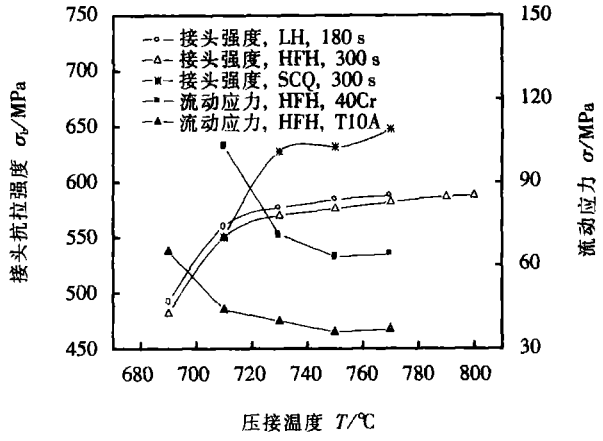

图 2 焊接温度与接头强度的关系

Fig. 2 Relationship between welding temperature and tensile strength of joint

(预压应力 $\sigma_0=56.6$ MPa,初始应变速率 $\dot{\varepsilon}_0=2.5\times10^{-4}\ s^{-1}$;应变 $\varepsilon=0.15$)

组织，而后者淬火区以外为供应态的退火组织。在拉伸试验时，同样断在接头区外的母材 40Cr处，前者显然具有较大的抗拉强度。在相同超塑压缩变形条件下 T10A比 40Cr具有较小的超塑流动应力（超塑均匀变形时对应的流动应力，见图 2，应变 $\varepsilon=0.15$）和较大的应变速率敏感性指数 m，见式（1）、（2）[9]，这是导致不同预处理情况下压接试样的 T10A侧径向变形（膨胀率）高于 40Cr侧径向变形（膨胀率）的原因。

初始应变速率，一般处在待焊双方最佳超塑应变速率范围的上限。初始应变速率与接头强度的关系见图 3，由图 3可见，焊接前组织的细化效果愈好，则达到 40Cr母材强度 ISSW 的实际初始应变速率向高应变速率区域移动。

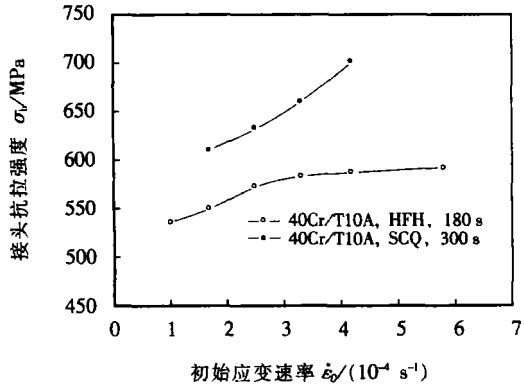

图 3　初始应变速率与接头强度的关系

Fig. 3　Relationship between initial strain rate and tensile strength of joint

（预压应力 σ_0=56.6 MPa，压接温度 T=750 ℃）

压接时间，在 ISSW 过程中，接头强度与时间的变化规律均近似于幂规律（图 4）。如果压接时间过短，接合面就会残存空隙致使焊接接头断在接口处。从图 4和表 3可见，一般需几分钟即可使接头强度达到 40Cr母材的强度，延长压接时间对接头强度几乎无影响，这与一般需要几十分钟的扩散焊接过程相比要短得多。由 SCQ→HFH→LH，40Cr/T10A 异材 ISSW 接头达到 40Cr钢母材强度所需时间明显缩短（由约 360 s→约 180 s→约 90 s），这佐证了晶界在超塑性及 ISSW 中所起的重要作用[2]，即随着焊接前组织的细化，以晶界滑移为主的材料超塑性效应更明显，其流动应力 σ 减小、应变速率敏感性指数 m 值升高、超塑压缩变形激活能 Q_c 降低，见式（1）、（2）；另一方面较细的晶粒为原子提供了更多的快速扩散的"通道"，扩散系数越大[2]。因此，焊前组织的超细化，有利于形成冶金结合所需的塑性流变和扩散，因而更容易实现焊合。

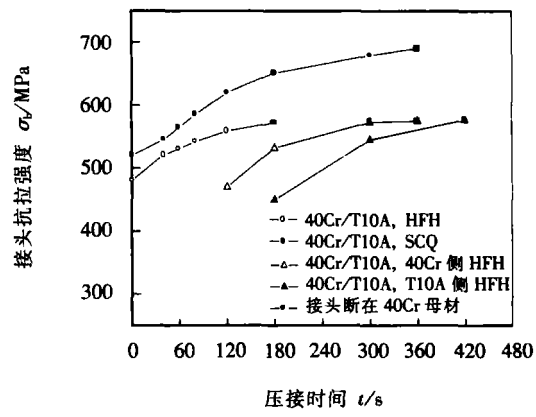

图 4　ISSW过程中接头强度变化

Fig. 4　Tensile strength of joint in process of ISSW

（预压应力 σ_0=56.6 MPa，压接温度 T=750 ℃；初始应变速率 $\dot{\varepsilon}_0=2.5\times10^{-4}$ s^{-1}）

表 3　不同工艺方案达到 40Cr母材强度所需时间（s）

Table 3　Times obtained to strength of 40Cr base metal in different technical projects

SCQ	HFH			LH
	HFH	40Cr侧 HFH	T10A侧 HFH	
360	约 180	300	420	约 90

$$\text{SCQ:}\begin{cases}\sigma_1=e^{-18.57}\dot{\varepsilon}^{0.34}\exp\left(\dfrac{209.9\times10^3}{RT}\right),\\ \sigma_2=e^{-17.29}\dot{\varepsilon}^{0.41}\exp\left(\dfrac{193.8\times10^3}{RT}\right),\end{cases}\quad(1)$$

$$\text{HFH:}\begin{cases}\sigma_1=e^{-17.44}\dot{\varepsilon}^{0.36}\exp\left(\dfrac{199.6\times10^3}{RT}\right),\\ \sigma_2=e^{-16.15}\dot{\varepsilon}^{0.43}\exp\left(\dfrac{183.6\times10^3}{RT}\right),\end{cases}\quad(2)$$

式中：σ_1、σ_2 分别为 40Cr钢、T10A钢的流动应力；m 值、Q_c 值均为所选温度区间（730～770 ℃）的平均值；$\dot{\varepsilon}$ 为 $\dot{\varepsilon}_0$/(10^{-4} s^{-1})。

与 ISSW 相比，U－ISSW（单边或单侧恒温超塑性固态焊接）可降低待焊双方之一的组织要求，尤其是对接头强度要求不太高时，它不仅简化了预处理工艺，更重要的是它可使一些不具备组织超塑性的材料实现 ISSW，具有开发应用价值。从图 4和表 3可见，由于单边或单侧超塑性，欲达到相同焊接效果，U－ISSW 比 ISSW 需要更长时间；在 ISSW 过程中，40Cr一侧的超塑效应对焊接效果具有更大的作用。

但在实际应用中，为实现较精密的 ISSW，需要控制变形量 ε，而 $\varepsilon\approx\dot{\varepsilon}t$，因此为获得可靠的 ISSW 接头，可选用不同的压接时间 t和应变速率 $\dot{\varepsilon}$搭配，如较高的 $\dot{\varepsilon}$下压接时间短些、较低的 $\dot{\varepsilon}$下时间长些，

但在焊接生产中应用还是前者更适合。

2.3 接头区组织

通过对 40Cr/T10A 钢 ISSW (含 U-ISSW)接头显微组织形貌特征的观察和分析，认为接头中存在"界面超细晶区"、"过渡区"等组织特征区域。

界面超细晶区，是指在压接前的升温、保温和焊接过程中，界面接触处的两侧金属受塑性变形和超塑性变形作用而发生动态再结晶现象形成的等轴、细小的公共晶粒构成的冶金结合区域(见图 5)。界面接触处微区所受应力状态的不同，导致其塑性变形状态的不同而使焊接面各微区焊合状态是非均匀的，该区域一般≤ 2 μm。

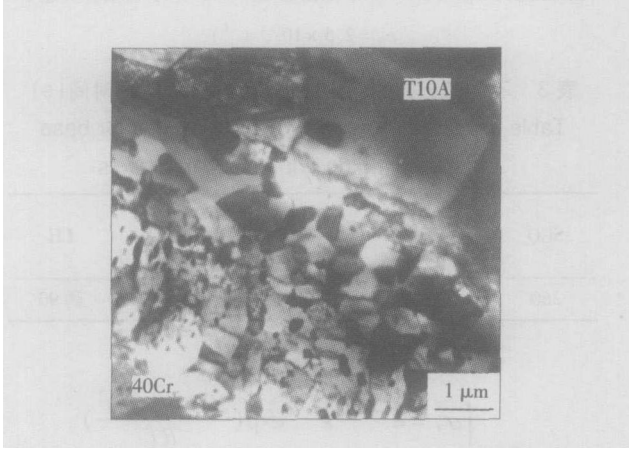

图 5 接头区界面处的 TEM 照片

Fig. 5 Interface microstructure of joint zone

过渡区，在界面两侧附近与远离界面的母材之间有一明显的组织过渡区。主要指在超塑效应作用下，近界面处(两侧)形成的扩散区，该区域的组织形态包括其中的碳化物数量、形态和分布等都发生了明显变化。T10A 侧，由于 C 向 40Cr 侧扩散而使 C 含量降低，在近界面 2 ~3 个晶粒宽的范围内，出现了平均尺寸为 2 ~3 μm 且晶内几乎无碳化物、近于等轴状的 α 晶粒(图 5右上方区域)，其显微硬度明显较低(该区域硬度约 200 HV0.1)；40Cr 侧，近界面处组织均为 α 晶粒及珠光体(α 基体内片状与粒状碳化物共存)的组织形态，α 晶粒平均尺寸明显较小(约 0.5 μm)，珠光体含量明显高于远离界面的 40Cr 母材，尤其是近界面的原 α/γ 相界及三叉晶界珠光体量更多。这表明 T10A 侧 C 原子向 40Cr 扩散，C 的扩散使 α 中 C 浓度升高即导致 γ 含量的增高而使珠光体量增多，这充分反映了晶界是原子扩散的快速通道。焊接前组织越细，ISSW 与 U-ISSW 相比，具有更宽的过渡区。

3 结 论

(1) 钢待焊表面组织对 ISSW 接头的形成有重要影响。焊接前钢的组织越细，ISSW 所需焊接温度向低温区移动，初始应变速率向高应变速率区域移动，ISSW 所需时间越短；即使待焊双方一方实施组织超细化，也可实现接头抗拉强度达到 40Cr 母材的强度，但 ISSW 所需压接时间稍长。

(2) ISSW 属小变形焊接。接头变形主要集中在原界面附近的淬火区，且 T10A 侧的变形均大于 40Cr 侧。

(3) ISSW 接头中存在着明显的"界面超细晶区"、"过渡区"等组织特征区域。

参考文献：

[1] 李志远，钱乙余，张九海. 先进连接方法[M]. 北京：机械工业出版社，2000. 1-4.

[2] 文九巴，杨蕴林，杨永顺，等. 超塑性应用技术[M]. 北京：机械工业出版社，2004. 181-208.

[3] Yang Yunlin, Li Zhi, Wen Jiuba, *et al*. Isothermal superplastic solid-phase welding of structural steel and tool steel[J]. Transactions of the China Institution, 1996, 17(1): 31-38.
杨蕴林，李 志，文九巴，等. 结构钢与工具钢的恒温超塑性固相焊接[J]. 焊接学报，1996，17(1)：31-38.

[4] Zhang K K, Yang Y L, Wang C S, *et al*. The superplastic solid-phase welding of 40Cr/T10A steel[J]. Journal of Materials Science & Technology, 2001, 17(1): 189-190.

[5] Ge Liling, Wang Min, Yao Zhekun, *et al*. Isothermal superplastic diffusion bonding of dissimilar steels[J]. Transactions of the China Welding Institution, 2000, 21(1): 75-78.
葛利玲，王 敏，姚泽坤，等. 异种钢的恒温超塑性扩散焊工艺[J]. 焊接学报，2000，21(1)：75-78.

[6] Zhang K K, Han C X, Quan S L, *et al*. Superplastic solid state welding of steel and copper alloy based on laser quenching of steel surface[J]. Trans. Nonferrous Met. Soc. China, 2005, 15(2): 384-388.

[7] Yang Yunlin, Ma Feng, Wang Changsheng, *et al*. Solid-phase welding between chromium bronze and wolfram alloy based on superplasticity of chromium bronze[J]. Transactions of the China Welding Institution, 2001, 22(2): 15-18.
杨蕴林，马 峰，王长生，等. 基于铬青铜超塑变形的铬青铜/钨合金固相焊接[J]. 焊接学报，2001，22(2)：15-18.

[8] YB/T 5148-1993, 金属平均晶粒度测定法截线法[S].

[9] Zhang K K, Yang Y L, Liu S Z, *et al*. Constitute equations of 40Cr steel under superplastic compressive deformation[J]. Acta Metallurgica Sinica, 2003, 16(6): 538-542.

作者简介：张柯柯，男，1965 年 2 月出生，工学博士，教授，国际焊接工程师(IWE)。主要从事新材料连接与特种连接技术、微电子连接用无铅钎料及其焊接性等方面的研究工作。先后主持参与完成省部级科研项目 10余项，发表论文 70余篇。

Email: zhkeke@mail.haust.edu.cn

ture toughness test standard. δ – R resistance curve tests were conducted with multiple specimens at 5 ℃ in welded joints of X56 pipeline steel. And then the $\delta_{0.2}$ values of weld and HAZ were obtained. The assessment was carried out by using the maximum stress at different water depth and the stress concentration and residual stress were also considered. The tolerable surface flaw sizes were gained at perfect alignment and maximum allowable misalignment. This study lays the foundation for judging the acceptability of flaws.

Keywords: British standard; tolerable size; engineering critical assessment

Finite element analyses of instantaneous stresses of hot plate welded joint of plastic pressure pipes WANG Jian-ping[1], HUO Li-xing[1], GU Kan-feng[2] (1. School of Materials Science and Engineering, Tianjin University, Tianjin 300072, China; 2. Shenyang Institute of Automation, Chinese Academy of Sciences, Shenyang 110015, China). p21 – 25

Abstract: Based on constitutive relationship of thermal viscoelastic integral mode, considering the properties of material which depend great on temperature fluctuation and the effect of phase transition latent heat, heat-force coupling function and load step character of ANSYS were employed to simulate the hot plate welding procedure of high density polyethylene (HDPE) plastic pressure pipe. The finite element analyses on stresses distribution of welded joint was conducted, and transient stresses distribution pattern in axial, radial and circumferential directions were obtained. Residual stresses was measured by the matharm method and the sachs method, and it showed that the actual measured results of the residual stresses are basically coincident with the results of numerical analysis.

Keywords: high-density polyethylene; pressure pipe; hot plate; welded joint; instantaneous stress; finite element analyses

Effect of single component fluoride flux on TIG arc shape for Ti alloy LI Xiao-hong, ZHANG Lian-feng, DU Yu-xiao (Beijing Aeronautical Manufacturing Technology Research Institute, Beijing 100024, China). p26 – 28

Abstract: BT20 titanium alloy of 2.5 mm thickness was welded by conventional TIG and single-component fluoride flux TIG, respectively. The results showed that the influences of different single-component fluorides on the shape of arc are different. And the relationship of arc shape and the weld penetration was also obtained.

Keywords: single-component fluoride flux; A-TIG welding; arc shape

Edge detection of weld image based on Canny operator XIE Zhi-meng, GAO Xiang-dong (Department of Mechanical and Electrical Engineering, Guangdong University of Technology, Guangzhou 510090, China). p29 – 32, 36

Abstract: Weld edge is the most important characteristic in a weld image. The fact of selecting an appropriate edge-detecting operator and obtaining the accurate weld edge information is a key process in weld image processing. The canny operator was used to extract the weld edge, and its principle and implementation were discussed. And the canny operator, kirsch operator, prewitt operator, robert operator, sobel operator and gauss-laplace operator were applied in detecting the weld edges to test the effects respectively. The analyzsis of the weld image and weld center coordinates showed that the canny operator is a very effective way to detect the weld edge, and also suitable for the seam-tracking process based on vision sensors.

Keywords: Canny operator; edge detection; seam tracking; image processing

Numerical simulation of improving welding efficiency of TIG surface protection ZHENG Shu[1], HU Guo-hui[1], CHEN Fang-quan[2], YANG Huan-ming[3] (1. Shanghai Institute of Applied Mathematics and Mechanics, Shanghai University, Shanghai 200072, China; 2. College of Manufacturing Automation, Shanghai University, Shanghai 200436, China; 3. Jian Zhong Chemicals Corporation, Sichuan Yibin 644000, China). p33 – 36

Abstract: Based on the Navier-Stokes equation and renormalization group (RNG) κ-ε turbulence model, the flows around the nuclear fuel stick and the weld cavity were simulated numerically by the SIMPLEC algorithm. The body-fitted coordinates, staggered grid method and self-adaptive technique was utilized in this study. Through the analysis of flow around the nuclear fuel stick and the weld cavity, the defect of the old structure was found out, and two methods to improve the welding efficiency were proposed.

Key words: computational fluid dynamics; nuclear fuel stick; SIMPLEC algorithm

Superplastic solid-state welding of dissimilar steels under different microstructure by ultra-fining treatment ZHANG Ke-ke[1], YANG Yun-lin[1], ZHAO Ning[2], WANG Chang-sheng[1], WANG Yao-li[1] (1. Material Science and Engineering College, Henan University of Science and Technology, Henan Luoyang 471003, China; 2. School of Material Science and Engineering, Xi'an Jiaotong University, Xi'an 710049, China). p37 – 40

Abstract: The microstructures of 40Cr and T10A steel and its surfaces were ultra-fined through salt bath cyclic quenching, high frequency hardening and laser hardening, then influence of the welded surface microstructure of steels on the process and joint quality of isothermal superplastic solid state welding (ISSW) for 40Cr/T10A dissimilar steels was studied. The experimental results showed that the welded surface microstructure of steel plays an important role in the formation of ISSW joint. The welding temperature of ISSW extends to low temperature ranges and the initial strain rate extends to higher strain rate ranges while having finer

welded surface microstructure of steel before welding. If only one surface is eligible for ultra-fining, the tensile strength of the joint will be also up to that of 40Cr base metal, but the welding time is slightly longer. ISSW belongs to the little deformation welding, the deformation of joint is mainly located in the quenched area near original interface. The deformation of T10A side is larger than that of 40Cr side.

Key words: steel; microstructure; ultra-fining treatment; superplastic solid-state welding; process

Phase transformation diffusion bonding technology for titanium alloy to stainless steel QIN Bin[1], SHENG Guang-min[1,2], HUANG Jia-wei[1], LI Cong[2] (1. College of Material Science and Engineering, Chongqing University, Chongqing 400044, China; 2. National Key Laboratory for Nuclear Fuel and Material, Nuclear Power Institute of China, Chengdu 610041, China). p41 - 44, 48

Abstract: The joints of titanium alloy (TA17) and stainless steel (0Cr18Ni9Ti) were obtained by phase transformation diffusion bonding. Effect of parameters on strength of the joint was investigated, and the optimum parameters for bonding are as follows: maximum cyclic temperature is 890 ℃, minimum cyclic temperature is 800 ℃, number of cyclic times is 10, bonding pressure is 5 MPa and heating velocity is 30 ℃/s. Strength of the joint under the optimum condition is 307 MPa, and the time for bonding is 160 s. Scanning electron microscopy (SEM), energy dispersive spectroscopy (EDS) and X-ray diffraction (XRD) were used to study the fracture appearance of the joint. The study showed that the fracture takes place at somewhere between FeTi and β-Ti layers, and the FeTi layer is the weakest point in the joints. The joint was analyzed by EDS and the ternary phase diagram for Fe-Cr-Ti. The results indicated the presence of σ, Fe_2Ti, FeTi and β-Ti in the reaction zone between stainless steel and titanium alloy.

Key words: titanium alloy; stainless steel; phase transformation; diffusion bonding

Metal transfer of twin-wire indirect arc argon welding CAO Mei-qing, ZOU Zeng-da, DU Bao-shuai, QU Shi-yao, WANG Xin-hong, LI De-gang (School of Material Science and Engineering, Shandong University, Jinan 250061, China). p45 - 48

Abstract: The metal transfer and the corresponding arc voltage and welding current in twin-wire indirect arc argon welding was investigated with high speed camera system based on a xenon lamp source and digital oscillograph. Results showed that with the different matching of welding current and arc voltage, the mode of metal transfer consists of short circuiting transfer, globular transfer, mixing transfer, projected transfer and streaming transfer etc. With the increasing of welding current, the droplet size reduces, and the droplet is refined. With the raising of arc voltage, the size of droplet reduces. There is well corresponding relationship between metal transfer mode and the oscillogram of volgtage and welding.

Key words: indirect arc; metal transfer; short circuiting transfer; streaming transfer

Autonomous seam tracking based on local vision in arc robotic welding ZHOU Lü, CHEN Shan-ben, LIN Tao, CHEN Wen-jie (Welding Institute, Shanghai Jiaotong University, Shanghai 200030, China). p49 - 52

Abstract: A method of autonomous seam tracking in arc robotic welding was presented. It could make the robot get rid of traditional teaching and playing back mode and automatically acquired the special coordinates of welding seam. The master computer continuously processed local area images in front of the torch in the images which were acquired by a CCD camera to measure the deviation between the torch and the seam and the orientation of the seam. At the same time, the computer controlled the robot to make the torch move forward along the seam and recorded the seam's coordinates in the robotic basic reference frame which were corrected by the deviations. After the torch arrives at the end-point of the seam, the computer controlled the robot to move the torch to the first record coordinate and begin to weld. Experiments were made on the curves seam workpieces of mild steel and aluminum alloy workpieces. The result showed that this method has good practicability.

Key words: image processing; arc welding robot; autonomous seam tracking; local vision

Distribution of Au during reaction of eutectic SnPb solder and Au/Ni/Cu pad LI Fu-quan[1], WANG Chun-qing[1], DU Miao[2] (1. National Key Laboratory of Advanced Welding Production Technology, Harbin 150001, China; 2. Harbin Welding Institute, Harbin 150080, China). p53 - 56

Abstract: Solder bump was fabricated with Sn-Pb eutectic solder droplet on Au/Ni/Cu pad. The solder/pad was then subject to reflow soldering and aging at 125 ℃. The IMC evolution at solder/pad interface during this process, especially the formation and distribution of Au-Sn compound were investigated. The results showed that Au-Sn compound forms at solder/pad interface during contact reaction, and Au does not react fully with solder droplet. During the subsequent reflow soldering, all Au layer at interface is consumed. Ni layer reacts with solder, which leads to the formation of Ni_3Sn_4 compound at the interface. Acicular $AuSn_4$ can be found in the solder bulk. $AuSn_4$ particles redesposites at the interface as a continuously $(Au_xNi_{1-x})Sn_4$ layer during aging at 125 ℃. The redesposited $(Au_xNi_{1-x})Sn_4$ at solder/pad interface follows decomposition-diffusion mechanism. At the same time, a lead-rich phase emerges with $AuSn_4$ redeposition at the interface. The shear strength of soldered joint is mainly determined by this evolution and distribution of Au-Sn compound.

Key words: solder bump; Au/Ni/Cu; reflow; ageing; interme